Indirect nuclear exchange coupling and electronic structure of the layered semiconductor TlS: NMR study and band structure calculation

2004 J. Phys.: Condens. Matter 16 3071

(http://iopscience.iop.org/0953-8984/16/18/008)

INSTITUTE OF PHYSICS PUBLISHING JOURNAL OF PHYSICS: CONDENSED MATTER

J. Phys.: Condens. Matter **16** (2004) 3071–3080 PII: S0953-8984(04)73457-8

Indirect nuclear exchange coupling and electronic structure of the layered semiconductor TlS: NMR study and band structure calculation

A M Panich[1,3] **and S Kashida**[2]

[1] Department of Physics, Ben-Gurion University of the Negev, PO Box 653, Beer Sheva 84105, Israel
[2] Department of Environmental Science, Faculty of Science, Niigata University, Ikarashi Ninocho 8050, Niigata 950-2181, Japan

E-mail: pan@bgumail.bgu.ac.il

Received 15 December 2003
Published 23 April 2004
Online at stacks.iop.org/JPhysCM/16/3071
DOI: 10.1088/0953-8984/16/18/008

Abstract

We have studied the electronic structure of the layered semiconductor TlS by means of ^{203}Tl and ^{205}Tl NMR and band structure calculation. The crystal structure of this compound is built from the metal–chalcogen layers formed of linked $Tl^{3+}S_4^{2-}$ tetrahedra and Tl^+ ions located between the layers. Our experiments show significant interlayer indirect exchange coupling of thallium nuclei. Since the distances between thallium ions essentially exceed the sum of their ionic radii, it is concluded that such coupling is realized due to the overlap of the Tl electron wavefunctions across the intervening S atom. The exchange interaction has been evaluated by means of the quantitative spectral analysis. The band structure calculation shows that the top of the valence band is composed of mixed Tl^+ $6s6p_z$–S $3s3p_z$–Tl^{3+} $6s6p_z$ states, yielding overlap of the Tl^+–S–Tl^{3+} type. Such electronic structure gives rise to the effective interlayer coupling of Tl nuclear spins observed in the experiment. This effect is discussed along with the recently obtained NMR results in the chain thallium sulfide and selenide.

1. Introduction

Thallium monosulfide is a mixed valence compound, represented by the formula $Tl^+Tl^{3+}S_2^{4-}$. This compound crystallizes in two different structures of the chain and layered type, respectively [1–5]. Tetragonal structure of the chain TlS [1] comprises alternating chains of uni- and trivalent thallium ions along the *c* axis. The layered modification of TlS [3–6], studied in

[3] Author to whom any correspondence should be addressed.

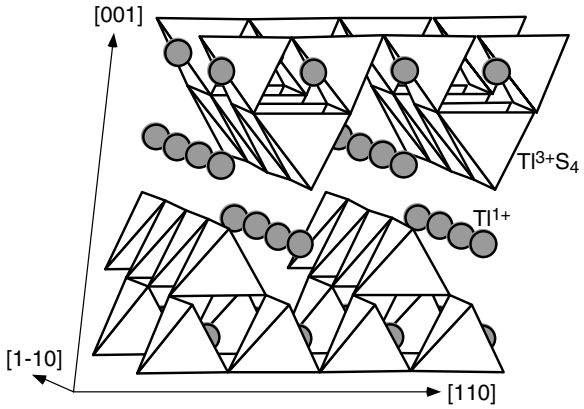

Figure 1. Layered structure of the monoclinic modification of TlS. Tl^+ ions (circles) are located between the layers formed by linked $Tl^{3+}S_4^{2-}$ tetrahedra.

this paper, is built from the metal–chalcogen layers formed of corner-linked $Tl^{3+}S_4^{2-}$ tetrahedra (figure 1). Univalent thallium atoms are located between the layers forming linear chains in the a, b-plane. The compound belongs to the $TlMX_2$ (M = Tl, Ga, In, X = S, Se) family, that is of great interest due to the low dimensionality, photoconductivity, semiconducting properties and potential applications for opto-electronic devices. Layered TlS undergoes successive phase transitions at 318 and 341 K with an intermediate incommensurate phase [3, 7, 8]. The structure of the low temperature phase belongs to the space group $C2$: $a = 11.018$, $b = 11.039$, $c = 4 \times 15.039 = 60.16$, $\beta = 100.77$ [3–5].

TlS is known as a semiconductor and shows good photoconductive properties [9]. However, its electronic structure has not been determined. Qualitative analysis of the photoemission spectra [9] allowed us to suggest that the inner valence band is derived from the Tl^{3+} 6p, Tl^{3+} 6s and the S 3p states forming strong sp^3-type bonding and antibonding states, and the top of the valence band contains hybrid orbitals of Tl^+ ions and the surrounding S^{2-} ions which are mainly S 3p and Tl^+ $6s^2$ lone pair orbitals. In this paper, we have studied the electronic structure of the layered TlS by means of ^{203}Tl and ^{205}Tl nuclear magnetic resonance (NMR) and band structure calculation. More specifically, we report on experimentally observed indirect exchange coupling among thallium nuclei due to the interlayer overlap of the Tl^+ and Tl^{3+} electron wavefunctions across the intervening chalcogen atom, in contrast with the expected two-dimensional behaviour of the compound. The effect is well confirmed by the band structure calculation. Both inter- and intra-layer couplings have been evaluated by means of the quantitative spectral analysis. The observed overlap is the important mechanism in the formation the uppermost valence bands and lower conduction bands in the electronic structure of the compound. Furthermore, we note that our recent thallium NMR study of the *chain* semiconductors TlSe [10] and TlS [11] showed significant indirect exchange coupling among thallium nuclei due to the *interchain* overlap of the Tl wavefunctions across the chalcogen atom. Similarity of such effects in thallium semiconductor chalcogenides is briefly discussed.

2. Experimental details

^{203}Tl and ^{205}Tl NMR measurements of powder TlS sample were performed using a Tecmag pulse NMR spectrometer. The NMR spectra were measured in the external magnetic fields B_0 from 0.87 to 1.30 T using a Varian electromagnet and $B_0 = 8.0196$ T using an Oxford

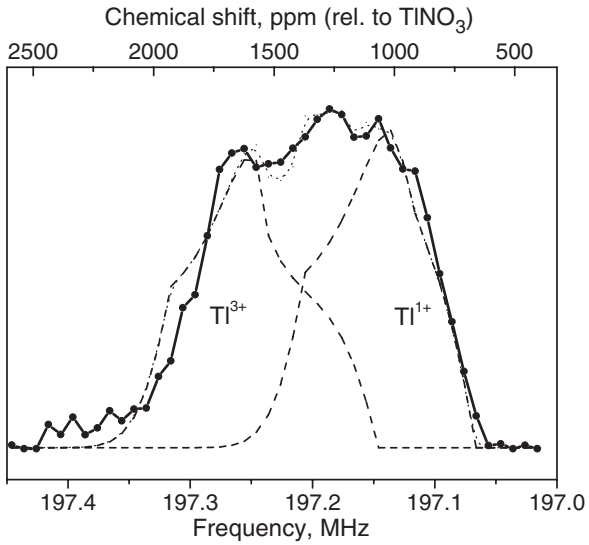

Figure 2. Experimental ^{205}Tl NMR spectra of the powder sample of TlS in the magnetic field $B_0 = 8.0196$ T (solid curve) and calculated spectra of the Tl^{+} and Tl^{3+} components (dashed curves). The total calculated spectrum is shown by the dotted curve.

superconducting magnet. The corresponding resonance frequencies of ^{205}Tl isotope are 21.4–32.1 and 197.2 MHz, respectively. The measurements have been made in the low temperature phase, at $T = 200$ K in order to be far from the phase transition to the incommensurate phase. In low magnetic field, the $\pi/2$ pulse was 2.2 μs, and the spectra were obtained from the Fourier transform of the spin echo. In high magnetic field, thallium NMR spectra cover a range of several hundred kilohertz and cannot be excited by a single $\pi/2$ pulse. Therefore the spectra (figure 2) were measured point by point with the echo sequence using frequency sweep technique [12–14]. Thallium NMR shifts are given relative to an aqueous 0.002 mol dm^{-3} solution of $TlNO_3$, the position of which is assigned to the value of 0 ppm.

3. Band structure calculations

The band structure calculations have been made using the full-potential linear-muffin-tin-orbital (LMTO) program 'LMTART' [15], where the local density approximation (LDA) is employed. As the base functions, s, p and d orbitals are taken for each atom. Multiple-k LMTO basis sets are used with two energy panels, one at -1.36 eV, and another at -13.6 eV. The space is divided into muffin-tin spheres and the interstitial region. The muffin-tin spheres are taken as large as possible without overlapping; the sphere's radii are adjusted so that the boundary potential values are not much different for different atoms. Inside the muffin-tin spheres, the wavefunction and potential are expanded using spherical harmonics. In the plane wave method used in this study, the wavefunction and potential are Fourier transformed in the interstitial region, where $48 \times 48 \times 92$ meshes are utilized. Since the room temperature structure of monoclinic TlS contains too many atoms in the unit cell ($Z = 144$), the present calculation was made for the prototype structure which is stable above 341 K and having the space group $C2/c$: $a = 11.02$, $b = 11.04$, $c = 15.04$ Å, $\beta = 100.69°$, $Z = 32$. The only difference between these structures is that the former shows a quadrupling of the period along the c axis in comparison to the latter.

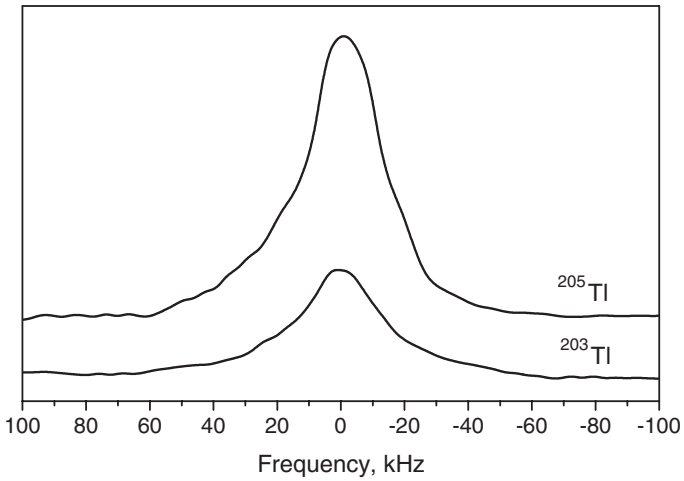

Figure 3. ^{205}Tl and ^{203}Tl NMR spectra of TlS at resonance frequency 21.4 MHz ($B_0 = 0.8710$ and 0.8796 T, respectively). Spectra are normalized to the number of scans.

4. Results of the experiments

The experimental ^{205}Tl NMR spectrum at resonance frequency 197.2 MHz is given in figure 2. Monoclinic symmetry of the thallium sites should correspond to a nonaxially symmetric chemical shielding (CS) tensor,

$$\sigma = \sigma_{11}\cos^2\varphi\sin^2\theta + \sigma_{22}\sin^2\varphi\sin^2\theta + \sigma_{33}\cos^2\theta. \tag{1}$$

Here φ and θ are the Euler angles of the magnetic field in the frame of the principal axes of the CS tensor. As well known, the powder line shape $f(\nu)$ corresponding to the nonaxially symmetric CS tensor is described by elliptic integrals [16, 17]. The calculated spectrum $F(\nu)$ is taken as a convolution of $f(\nu)$ with a Gaussian broadening function. The experimental spectrum was fitted by a superposition of two $F(\nu)$ lines corresponding to the Tl^+ and Tl^{3+} ions. The calculated spectra are also shown in figure 2. The fit yields $\sigma_{11}(Tl^+) = 690$ ppm, $\sigma_{22}(Tl^+) = 995$ ppm, $\sigma_{33}(Tl^+) = 1421$ ppm, and $\sigma_{11}(Tl^{3+}) = 1112$ ppm, $\sigma_{22}(Tl^{3+}) = 1589$ ppm, $\sigma_{33}(Tl^{3+}) = 1970$ ppm. The corresponding values of the tensor's traces are $\sigma_i(Tl^+) = 1035$ ppm, $\sigma_i(Tl^{3+}) = 1557$ ppm. The accuracy in evaluation of the CS components is 20 ppm. According to the thallium CS scale [18], the Tl^{3+} ion shows downfield resonance in comparison to Tl^+. Thus the resonance at $\sigma_i = 1035$ ppm was attributed to Tl^+, while the resonance showing $\sigma_i = 1557$ ppm was attributed to Tl^{3+}.

Let us now consider ^{203}Tl and ^{205}Tl spectra at low resonance frequencies, $\nu_0 = 21.4$–32.1 MHz. All these spectra are broad singlet lines (figure 3). At $\nu_0 = 21.4$ MHz, their line widths $\Delta\nu(^{203}\text{Tl}) = 27.5$ and $\Delta\nu(^{205}\text{Tl}) = 26$ kHz and second moments $M_2(^{203}\text{Tl}) = 420$ and $M_2(^{205}\text{Tl}) = 350$ kHz^2 are much larger than those resulting from the contributions of the dipole–dipole interactions of nuclear spins. The latter are estimated from the structure of TlS as $M_{2\text{dd}} \sim 1.2$ kHz^2. The contribution of the chemical shielding anisotropy to the second moment, calculated as $M(\Delta\sigma) = 46$ kHz^2 at the resonance frequency 21.4 MHz, is also smaller than the M_2 values obtained. This means that another mechanism determines the line shape. As known, the NMR spectra in most Tl-containing compounds are strongly caused by significant indirect exchange interactions among Tl isotopes [10, 11, 17, 19–22]. Van Vleck has shown [23] that exchange interaction J_{jk} between like and unlike spins yields different

contributions to the width and second moment of the NMR line. In the crystal that contains two different types of atom (or isotope) having spins I and I', the exchange contribution to the second moment of the unprimed spins, which are assumed to be responsible for the resonance absorption at the utilized frequency, is given by

$$M_2 = \tfrac{1}{3} I'(I'+1) \sum_{k'} J_{jk'}^2 \tag{2}$$

with the sum on the primed spins only. Therefore the ratio of the second moments of two different isotopes is inversely proportional to the ratio of their natural abundances. The two thallium isotopes are unlike since they have different gyromagnetic ratios. Their natural abundances are $f = 29.5\%$ for ^{203}Tl and $(1-f) = 70.5\%$ for ^{205}Tl, that should yield $M_2(\mathrm{Tl}^{203})/M_2(\mathrm{Tl}^{205}) = (1-f)/f = 2.39$. For structurally equivalent thallium atoms, nuclear exchange of the ^{205}Tl–^{205}Tl and ^{203}Tl–^{203}Tl types (like spins) leads to the exchange narrowing of the corresponding resonances, while the ^{203}Tl–^{205}Tl exchange coupling (unlike spins) yields the second moment increase (i.e. broadening) of both ^{203}Tl and ^{205}Tl resonances.

The obtained Tl signals are indeed characteristic for the indirect exchange coupling among nuclei [10, 11, 17, 19–22]. However, the experiments show that the line widths of ^{203}Tl and ^{205}Tl isotopes are close to each other. The experimental ratio of the second moments of ^{203}Tl and ^{205}Tl isotopes at 21.4 MHz is 1.2 instead of 2.39. It means that the indirect exchange between structurally inequivalent Tl^+ and Tl^{3+} ions plays a significant role and possibly dominates over the Tl^{3+}–Tl^{3+} and Tl^+–Tl^+ exchange. In such a case, line broadening is expected not only for ^{203}Tl–^{205}Tl but also for $^{205}Tl^+$–$^{205}Tl^{3+}$ and $^{203}Tl^{1+}$–$^{203}Tl^{3+}$ exchange interactions, while the exchange narrowing results only from the $^{205}Tl^+$–$^{205}Tl^{1+}$, $^{203}Tl^{1+}$–$^{203}Tl^{1+}$, $^{205}Tl^{3+}$–$^{205}Tl^{3+}$ and $^{203}Tl^{3+}$–$^{203}Tl^{3+}$ interactions. Therefore, the $M_2(\mathrm{Tl}^{203})/M_2(\mathrm{Tl}^{205})$ ratio differs from 2.39. (We note that the natural abundance of the ^{39}S isotope is 0.74% and thus Tl–S interaction is negligible.)

Moreover, one can see that instead of two lines expected for the two structurally inequivalent sites occupied by the trivalent and univalent thallium ions, the single ^{203}Tl and ^{205}Tl resonances were obtained at resonance frequencies up to 32.1 MHz. This fact also allows us to suggest a significant exchange interaction $J_{13} I_1 I_3$ between nuclei of Tl^+ and Tl^{3+} ions that leads to a collapse of their resonance lines. It is well known that NMR spectra of exchange-coupled nuclei strongly depend on the ratio of the exchange constant J and NMR frequency separation between two sites δ [24, 25]. The collapse of lines occurs at $\delta/J_{13} = 2\sqrt{2}$. Using the above value of $\delta = (\sigma_{3\iota} - \sigma_{1\iota}) = 522$ ppm and $\nu_0 = 32.1$ MHz, one can estimate that the Tl^+–Tl^{3+} exchange interaction $J_{13} > 6$ kHz.

When two resonances are collapsed, the line width is the average of the widths of Tl^+ and Tl^{3+} lines plus an extra part due to incomplete averaging of the two resonance frequencies. This additional broadening is proportional to δ^2 [24, 25]. Taking into account the contribution of the chemical shielding anisotropy $\Delta\sigma$ that occurs in a powdered sample, the full line width at half maximum height may be written as

$$\Delta\nu = \Delta\nu_0 + \Delta\sigma \times \nu + \delta^2\nu^2/(4J_{13}). \tag{3}$$

(We use here the field independent value of δ in units of ppm and ν in MHz, thus the spacing between signals in frequency units is $\delta \times \nu$; $\Delta\sigma$ is in ppm as well.) The experimental dependence of $\Delta\nu$ on the squared resonance frequency, measured in fields from 0.87 to 1.30 T, is given in figure 4. Analysis of this dependence using equation (3) yields $\Delta\nu_0 = 7.6$ kHz, and $J_{13} = 11.3$ kHz.

The exchange constants can be also calculated from the second moment values. Since both Tl isotopes have spin $I = 1/2$, and taking into account the contribution of the chemical

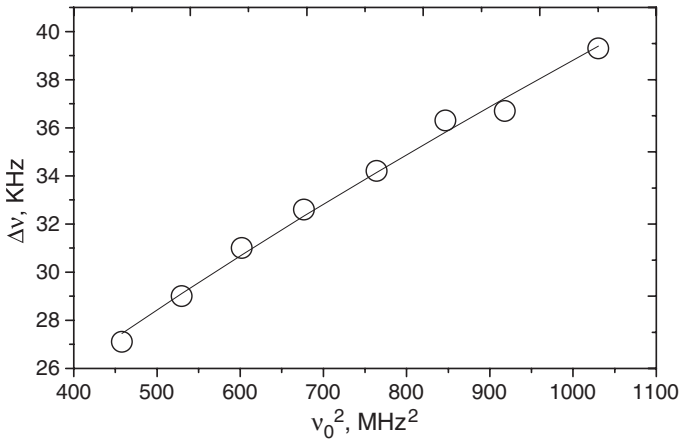

Figure 4. Experimental frequency dependence of ^{205}Tl NMR line width (open circles). The solid line shows a fit according to equation (3).

shielding anisotropy $M_2(\Delta\sigma)$, equation (2) is transformed to

$$M_2 = \tfrac{1}{4}(N_{11}J_{11}^2 + N_{33}J_{33}^2 + N_{13}J_{13}^2) + M_2(\Delta\sigma). \tag{4}$$

Here J_{11} and J_{33} are the Tl^+–Tl^+ and Tl^{3+}–Tl^{3+} exchange coupling constants, J_{13} is the Tl^+–Tl^{3+} exchange interaction and N_{11}, N_{33} and N_{13} are the numbers of nearest neighbours in Tl^+–Tl^+, Tl^{3+}–Tl^{3+} and Tl^+–Tl^{3+} structural fragments. In TlS, $N_{11} = 2$, $N_{33} = 4$ and $N_{13} = 6$, respectively. Using equation (4), from the two M_2 values for ^{203}Tl and ^{205}Tl isotopes one can calculate that $(J_{11}^2 + 2J_{33}^2)^{1/2} = 18.5$ kHz, and $J_{13} = 13$ kHz; the latter is close to that determined above from the frequency dependence of the line width. If one suggests that $J_{11} \approx J_{33}$, we find that $J_{11} = J_{33} = 10.7$ kHz.

5. Electronic band structure of the layered TlS

The calculated band structure of the layered semiconductor TlS is shown in figure 5. The lowest band around -13 to -12.5 eV comprises the S 3s states mixed somewhat with the Tl^{3+} 5d states. The band located around -11.5 to -10 eV is composed for the most part of the Tl^{3+} and Tl^+ 5d states and some contribution of the S 3s states. The main valence band is split into two sub-bands. The lower band, from -6.7 to -4.3 eV, consists of the Tl^{3+}, Tl^+ 6s–S 3s, 3p states. The upper band, from -4.0 to 0 eV, is composed mostly of the S 3p states with a smaller contribution of the Tl^+ 6s, 6p states; some even smaller contribution of the Tl^{3+} 6s, 6p states also occurs. The lowest part of the conduction band, below 4 eV, is composed in the main of the Tl^{3+} 6s, 6p, Tl^+ 6p and S 3p states. We note that the top of the valence band located at the Γ point is composed basically of Tl^+ 6s, $6p_z$–S $3p_z$–Tl^{3+} 6s, $6p_z$, $5d_{x^2-y^2}$ states in which the aforementioned wavefunctions are mixed into each other. The corresponding atomic orbital coefficients are given in table 1. One can find that the contribution of the Tl^+ 6s states exceeds that of the Tl^{3+} 6s ones. The bottom of the conduction band is composed mainly of Tl^{3+} 6s, $6p_z$–S 3s, $3p_z$–Tl^+ $6p_z$ mixed states (table 1). The contributions of Tl^+ 6s and Tl^{3+} $5d_{z^2}$ are also present; however, in contrast to the valence band, the Tl^{3+} 6s wavefunction dominates here over the Tl^+ 6s one. We note that the coefficients given in table 1 are the averaged values over 8 Tl^+, 8 Tl^{3+} and 16 S atoms. The calculation shows that the layered TlS is a direct gap semiconductor with the energy gap $E_g = 0.4$ eV. This is rather small compared with the experimental value

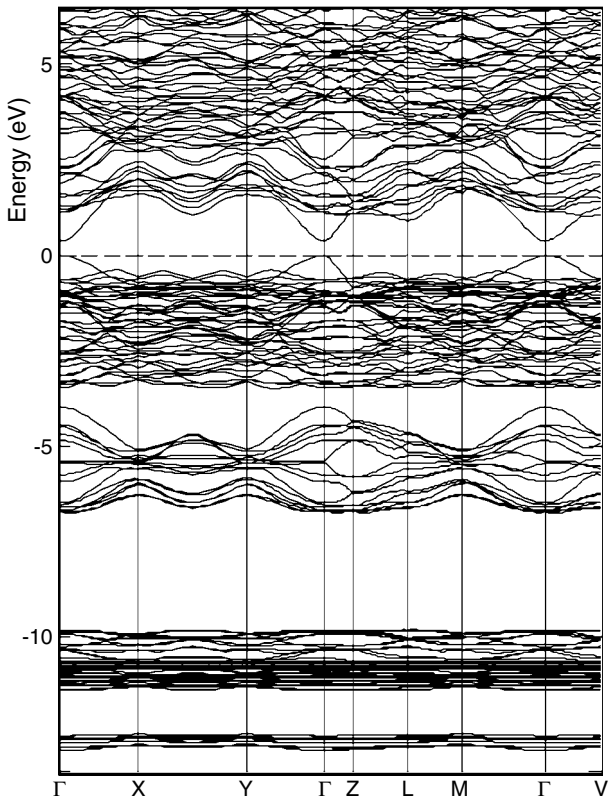

Figure 5. Band structure of the layered semiconductor TlS. The wavevectors of the symmetrical points are Γ, (0, 0, 0); X, $(2\pi/a, 0, 0)$; Y, $(0, 2\pi/b, 0)$; Z, $(0, 0, 2\pi/a)$; L, $(\pi/a, \pi/b, -\pi/c)$; M, $(2\pi/a, 0, -\pi/c)$; V, $(\pi/a, \pi/b, 0)$.

of 0.9 eV, which was estimated from the temperature dependence of the electrical conductivity in the intrinsic conduction region [9]. The observed LDA underestimate of the bandgap is an expected manifestation of the well known 'bandgap problem'. It is not substantial for the present analysis, since the LDA gives relatively correct eigenstates and wavefunctions.

6. Discussion

Formally spherically symmetric $5d^{10}6s^2$ and $5d^{10}$ electron configurations of the Tl^+ and Tl^{3+} ions in TlS could not yield the chemical shielding anisotropy (CSA) observed in the experiment. Thus one is led to consider sp hybridization of the Tl wavefunctions that yields a deviation from the spherical form of the Tl electronic charge distribution. The paramagnetic contribution to the chemical shielding

$$\sigma_{\mathrm{p}} \sim \Sigma \langle \psi_0 | L_z / r^3 | \psi_v \rangle \langle \psi_v | L_z | \psi_0 \rangle / \Delta E \tag{5}$$

that is responsible for CSA results from the mixing between the occupied ground state and the unoccupied excited states due to the partial unquenching of the orbital angular momentum L of the electrons in the applied magnetic field. Here ΔE is a suitable average of the energy difference between the conduction and the valence bands. Therefore, the main contribution to CSA comes from the states near the top of the valence band and the bottom of the conduction

Table 1. Wavefunctions and corresponding atomic orbital coefficients (a) at the top of the valence band and (b) at the bottom of the conduction band. Indices x, y and z correspond to the a, b and c axes shown in figure 1.

(a) Valence band top:								
				Tl^{+}				
6s	$6p_x$	$6p_y$	$6p_z$	$5d_{yz}$	$5d_{zx}$	$5d_{z^2}$	$5d_{xy}$	$5d_{x^2-y^2}$
0.153	0.002	0.002	0.031	0.000	0.000	0.000	0.002	0.015
				Tl^{3+}				
6s	$6p_x$	$6p_y$	$6p_z$	$5d_{yz}$	$5d_{zx}$	$5d_{z^2}$	$5d_{xy}$	$5d_{x^2-y^2}$
0.029	0.001	0.001	0.040	0.001	0.002	0.0142	0.001	0.060
		S^{2-}						
3s	$3p_x$	$3p_y$	$3p_z$					
0.022	0.0168	0.0168	0.173					
(b) Conduction band bottom:								
				Tl^{+}				
6s	$6p_x$	$6p_y$	$6p_z$	$5d_{yz}$	$5d_{zx}$	$5d_{z^2}$	$5d_{xy}$	$5d_{x^2-y^2}$
0.018	0.018	0.018	0.189	0.000	0.003	0.009	0.003	0.011
				Tl^{3+}				
6s	$6p_x$	$6p_y$	$6p_z$	$5d_{yz}$	$5d_{zx}$	$5d_{z^2}$	$5d_{xy}$	$5d_{x^2-y^2}$
0.151	0.006	0.006	0.018	0.002	0.004	0.018	0.004	0.007
		S^{2-}						
3s	$3p_x$	$3p_y$	$3p_z$					
0.093	0.020	0.020	0.097					

band. The band structure calculation (table 1) shows that these states are actually Tl^{3+}, Tl^{+} 6s6p–S 3s3p hybrid states, in good agreement with NMR data. A small contribution of the Tl 5d states located near the valence band top and conduction band bottom is also present. We note that NMR spectra of chain TlSe and TlS semiconductors [10, 11] also show CSA analogous to the compound under study. The CSA effects are larger in thallium selenide than in sulfides.

Indirect nuclear exchange in solids is realized due to overlap of the electron clouds of atoms. However, the Tl^{3+}–Tl^{3+}, Tl^{+}–Tl^{+} and Tl^{3+}–Tl^{+} distances, 3.95, 3.91 and 4.25 Å, respectively, essentially exceed the sum of the ionic radii of the Tl^{+} ($r = 1.59$ Å for CN = 8) and Tl^{3+} ($r = 0.75$ Å for CN = 4) ions and are therefore rather long to guarantee a significant Tl–Tl overlap. Since sulfur atoms are the first neighbours of Tl, one can conclude that indirect coupling of nuclei is caused by the electron cloud overlap of the Tl–S–Tl type. As shown by Bloembergen and Rowland [17], indirect exchange coupling of nuclei is put into effect via intermediate excited electronic states. It is realized by means of s parts of wavefunctions having a nonzero value $|\Psi(0)|^2$ at the nucleus site. Thus an assistance of Tl 6s states is necessary. The interaction between nuclear spins of atoms A and B is of the order of [17, 26]

$$|\Psi_{\mathrm{A}}(0)|^2 \times |\Psi_{\mathrm{B}}(0)|^2/\Delta E. \tag{6}$$

The main contribution comes therefore from the states at the top of the valence band and at the bottom of the conduction band. The band structure calculation shows that the valence band top and conduction band bottom are composed of the Tl^{+} $6s6p_z$–S $3s3p_z$–Tl^{3+} $6s6p_z$ mixed states, readily yielding the interlayer overlap of the Tl^{3+}–S–Tl^{+} type. Such electronic structure results in the effective exchange coupling of Tl nuclear spins observed in the experiment. Moreover, it

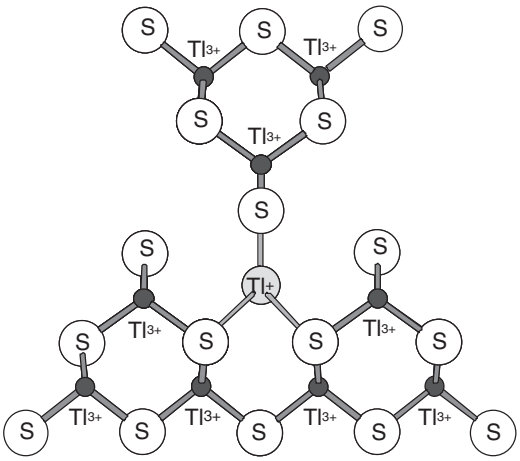

Figure 6. Arrangement of atoms around the Tl^+ ion showing one of the Tl^+–S–Tl^{3+} bonds in the TlS structure (view along the Tl^+ channel).

implies a formation of weak Tl^{3+}–S–Tl^+ chemical bonds by means of directed sp and p orbitals. One such bond in the TlS structure is shown in figure 6. The intralayer Tl^{3+}–S–Tl^{3+} coupling is evidently realized by means of the Tl^{3+}–S covalent bonds. (The average Tl^{3+}–S distance of 2.51 Å is in good agreement with the sum of the covalent radii of Tl (1.47 Å) and S (1.04 Å).) Thus we conclude that the experimental data on wavefunction hybridization and overlap are in good agreement with the band structure calculations. One can suggest that the interlayer overlap obtained should reduce the anisotropy of the physical properties of TlS in comparison to the layered semiconductors $A^{III}B^{VI}$.

We note that our recent thallium NMR study of the *chain* semiconductors TlSe [10] and TlS [11] showed significant indirect exchange coupling among thallium nuclei due to the *interchain* overlap of the Tl^+ and Tl^{3+} electron wavefunctions across the intervening chalcogen atom. The values of the exchange couplings in the chain and layered thallium monosulfides are of the same order; in TlSe they are larger than in TlS. This fact correlates with the relative ratios of CSA in TlSe and TlS mentioned above. One can suggest that the larger sp hybridization in thallium selenide results in larger overlap of its wavefunctions with those of the chalcogen atom. It seems that the aforementioned hybridization and overlap effect is a common property of thallium semiconductor chalcogenides.

7. Summary

In summary, our study of the layered semiconductor TlS by means of ^{203}Tl and ^{205}Tl NMR and band structure calculation shows significant interlayer indirect exchange coupling of thallium nuclei. Quantitative spectral analysis based on the frequency dependence of the line width and second moment values allows us to evaluate all coupling constants. Since the Tl–Tl distances essentially exceed the sum of the ionic radii of Tl, we conclude that such coupling is realized due to the overlap of the Tl electron wavefunctions across the intervening S atom. The band structure calculation shows that the top of the valence band is composed of mixed Tl^+ $6s6p_z$–S $3s3p_z$–Tl^{3+} $6s6p_z$ states, yielding overlap of the Tl^+–S–Tl^{3+} type. Such electronic structure results in the effective interlayer coupling of Tl nuclear spins observed in the experiment. Taking into account our studies of chain compounds TlSe and TlS, one can conclude that the aforementioned interchain/interlayer wavefunction overlap, which results in nuclear exchange, is a common property of thallium semiconductor chalcogenides.

References

[1] Hahn H and Klinger W 1949 *Z. Anorg. Allg. Chem.* **260** 110
[2] Ketelaar J A, Hart W H, Moorel R and Polder D 1939 *Z. Kristallogr.* **101** 396
[3] Kashida S, Nakamura K and Katayama S 1992 *Solid State Commun.* **82** 127
[4] Nakamura K and Kashida S 1993 *J. Phys. Soc. Japan* **62** 3135
[5] Kashida S and Nakamura K 1994 *J. Solid State Chem.* **110** 269
[6] Sardarly R M, Abdullaev A P, Guseinov G G, Nadzhafov A I and Eyubova N A 2000 *Crystallogr. Rep.* **45** 551
[7] Kashida S, Nakamura K and Katayama S 1993 *J. Phys.: Condens. Matter* **5** 4243
[8] Kashida S 1994 *Ferroelecrtrics* **151** 165
[9] Kashida S, Saito T, Mori M, Tezuka Y and Shin S 1997 *J. Phys.: Condens. Matter* **9** 10271
[10] Panich A M and Gasanly N M 2001 *Phys. Rev.* B **63** 195201
[11] Panich A M and Kashida S 2002 *Physica* B **318** 217
[12] Fukushima E and Roeder S B W 1981 *Experimental Pulse NMR: a Nuts and Bolts Approach* (Reading, MA: Addison-Wesley) p 45
[13] Vega A J, Farneth W E, McCarron E M and Bordia R K 1989 *Phys. Rev.* B **39** 2322
[14] Piskunov Yu, Gerashenko A, Pogulin A, Ananyev A, Mikhalev K, Okulova K, Verkhovskii S, Yakubovsky A and Trokiner A 2002 *Phys. Rev.* B **65** 134518
[15] Savrasov S V 1996 *Phys. Rev.* B **54** 16470
[16] Bloembergen N and Rowland T J 1953 *Acta Metall.* **1** 731
[17] Bloembergen N and Rowland T J 1955 *Phys. Rev.* **97** 1679
[18] Hinton J F, Metz K R and Briggs R W 1982 *Annual Reports of NMR Spectroscopy* vol 13, ed G A Webb (London: Academic) p 211
[19] Saito Y 1966 *J. Phys. Soc. Japan* **21** 1072
[20] Kholopov E V, Panich A M, Moroz N K and Kriger Yu G 1983 *Sov. Phys.—JETP* **57** 632
[21] Panich A M 1989 *Sov. Phys.—Solid State* **31** 1814
[22] Panich A M and Doert Th 2000 *Solid State Commun.* **114** 371
[23] Van Vleck J H 1948 *Phys. Rev.* **74** 1168
[24] Carrington A and McLachlan A D 1967 *Introduction to Magnetic Resonance* (New York: Harper and Row)
[25] Abragam A 1961 *The Principles of Nuclear Magnetism* (Oxford: Clarendon)
[26] Slichter C P 1992 *Principles of Magnetic Resonance* (Berlin: Springer)